

Surface-symmetry-driven Dzyaloshinskii–Moriya interaction and canted ferrimagnetism in collinear magnetoelectric antiferromagnet Cr_2O_3

Oleksandr V. Pylypovskiy,^{1,2,*} Sophie F. Weber,^{3,†} Pavlo Makushko,¹

Igor Veremchuk,¹ Nicola A. Spaldin,^{3,‡} and Denys Makarov^{1,§}

¹*Helmholtz-Zentrum Dresden-Rossendorf e.V., Institute of Ion Beam Physics and Materials Research, 01328 Dresden, Germany*

²*Kyiv Academic University, Kyiv 03142, Ukraine*

³*Materials Theory, ETH Zürich, Wolfgang-Pauli-Strasse 27, 8093 Zürich, Switzerland*

(Dated: October 20, 2023)

Antiferromagnets are normally thought of as materials with compensated magnetic sublattices. This adds to their technological advantages but complicates readout of the antiferromagnetic state. We demonstrate theoretically the existence of a Dzyaloshinskii–Moriya interaction (DMI) which is determined by the magnetic symmetry classes of Cr_2O_3 surfaces with an in-plane magnetic easy axis. The DMI explains a previously predicted out-of-plane magnetization at the nominally compensated surfaces of chromia, leading to a surface-localized canted ferrimagnetism. This is in agreement with magnetotransport measurements and with density functional theory predictions which further allow us to quantify the strength of DMI. The temperature dependence of the transversal resistance for these planes shows distinct behavior in comparison with that of the Cr_2O_3 c plane, which we attribute to the influence of DMI. Our work provides a framework to analyze surface-driven phenomena in antiferromagnets, and motivates the use of nominally compensated chromia surfaces for antiferromagnetic spintronics and magnonics.

Introduction. Chromia Cr_2O_3 is a rare example of a room temperature uniaxial magnetoelectric antiferromagnet (AFM) with the bulk Néel temperature $T_N = 308$ K. Beyond its potential in energy efficient AFM-based magnetoelectric data storage [1–3], this material offers a convenient platform for fundamental explorations of spin Hall physics [4, 5], THz magnetization dynamics [4], spin superfluidity [6] and electric-field-only manipulation of magnetism [2]. These studies build on the solid knowledge collected for the highest symmetry surface cut of chromia, terminated by the (001) surface (c plane) [7, 8] [Fig. 1(a)]. This surface hosts one AFM sublattice and features substantial magnetization perpendicular to the surface, whose sign is linked to the bulk Néel vector \mathbf{L} , proportional to the staggered sum of the individual magnetic moments $\mu_{1\dots 4}$ in the unit cell with odd and even indices belong to different AFM sublattices [7, 9]. This coupling enables all-electric access to the AFM order parameter using conventional magnetotransport methods. In contrast to the (001) surface, the coupling between $\mathbf{M} \propto \sum_i \mu_i$ and \mathbf{L} is symmetry-forbidden in bulk chromia. Bulk Cr_2O_3 does have a symmetry-allowed coupling between the primary order parameter \mathbf{L} and another antiferromagnetic vector, $\mathbf{L}_3 \propto \mu_1 + \mu_2 - \mu_3 - \mu_4$, due to an antisymmetric Dzyaloshinskii–Moriya interaction (DMI) [10, 11]. However, in the easy-axis ground state, $\mathbf{L}_3 \equiv 0$ and thus the bulk DMI and corresponding coupling vanishes [12].

The technological potential of thermodynamically stable chromia surfaces other than the c plane has not been explored, in part due to a lack of understanding of the surface magnetization and its link to the Néel vector. In particular, high-symmetry surfaces perpendicular to the c plane such as the a planes and m planes [Fig. 1(a)]

are magnetically compensated if the magnetic ordering at the surface does not deviate from the bulk. Thus, traditionally, the possibility of surface magnetization on these planes was not considered. However, recent experiments provide evidence for a sizeable spin transport and existence of finite magnetization in particular at the m plane (100) and a plane ($\bar{1}20$) of chromia [13–16], which could be highly relevant for magnonics and physical phenomena such as spin superfluidity because of the in-plane orientation of \mathbf{L} [6]. Furthermore, there is an active search for the uncompensated magnetization, which is coupled to the Néel vector [5, 16–18] and signature of DMI in non-collinear textures like domain walls in chromia [19].

This naturally brings attention to crystal surfaces, which are the primary source of interfacial DMI. In contrast to symmetry breaking at surfaces of ferromagnets, the surface-induced phenomena in AFMs are less well studied. Due to the lack of a complete theory of surface magnetism of AFMs, interpretation of magnetotransport, magnonics and spin-texture imaging experiments often interpolates from the behavior of bulk AFMs. This simplification can hide a broad family of fundamental effects. Recently, the surfaces of AFMs have started to attract attention, facilitated by the establishment of a portfolio of techniques that provide access to the relevant physics. These include magnetic circular dichroism [16], nitrogen vacancy magnetometry [3, 20, 21], magnetoelectric force microscopy [22], magnetotransport measurements [2, 23–26] as well as sophisticated theoretical methods combining first-principle and model calculations [3, 5, 8, 27–29].

Here, we demonstrate that the magnetic symmetry of the nominally compensated surfaces of Cr_2O_3 , i.e., m and a planes, provides a sizeable DMI that changes the mag-

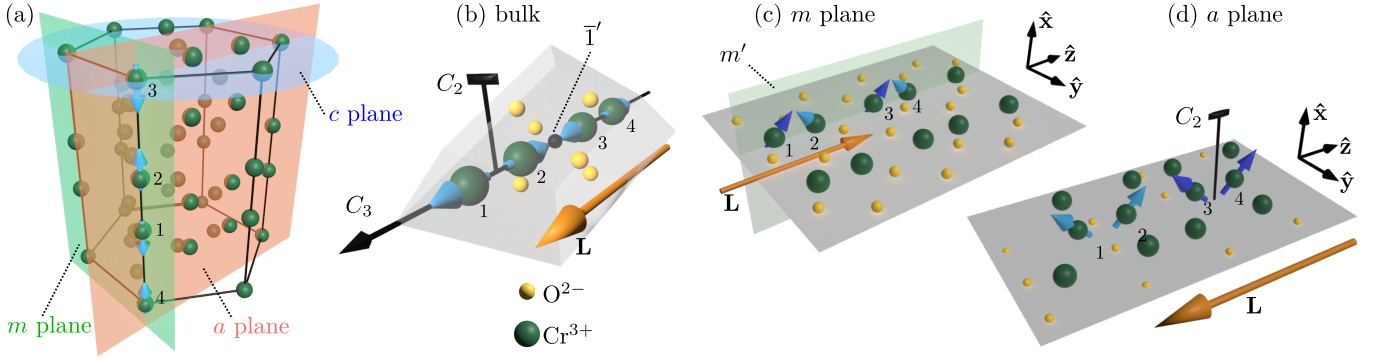


FIG. 1. **Bulk and surface symmetries.** (a) Cr atoms (green spheres) in the hexagonal cell of Cr_2O_3 . c plane (001), m plane (100) and a plane ($\bar{1}20$) are shown by the semitransparent blue, green and red planes, respectively. Blue arrows show directions of magnetic moments for the selected ions. (b) The basis of atoms in the bulk rhombohedral unit cell of Cr_2O_3 with the magnetic ordering $\{+ - + -\}$. Here, yellow and green spheres correspond to the O and numbered Cr ions, respectively. The yellow arrow indicates direction of the Néel vector \mathbf{L} . Three-fold and two-fold rotation axes C_3 and C_2 , respectively, are shown, $\bar{1}'$ corresponds to the center of anti-inversion. (c) Schematic of the m plane with the mirror plane m' . Inequivalent moments are shown by bright and dark blue arrows. Axis $\hat{\mathbf{x}}$ is parallel to the surface normal. (d) Schematics of the a plane with the two-fold rotation axis C_2 . Other notations same as in panel (c).

netic ordering at these surfaces and is responsible for the spin canting within the micromagnetic description of AFMs. The DMI is described and quantified using *ab initio* and micromagnetic approaches. Its physics can be understood in terms of the single-ion and inter-ion anisotropies, as well as antisymmetric exchange. In contrast to the interfacial DMI induced by the inversion symmetry breaking at interfaces [30, 31], the surface-symmetry-driven DMI relies on the change of the magnetic symmetry point group approaching the sample's surface from the bulk [32]. This DMI couples the primary Néel vector \mathbf{L} with magnetization \mathbf{M} , which is globally symmetry forbidden in bulk Cr_2O_3 . The coupling causes \mathbf{M} to switch with \mathbf{L} , providing all-electric access to \mathbf{L} for surfaces in which it lies in-plane. The temperature dependence of the transversal resistance shows that the thermodynamic properties of these surfaces differ from those of the c plane, which we attribute to the presence of DMI. Furthermore, we demonstrate that the surface-symmetry-driven DMI results in a change of the magnetic ordering from a collinear bipartite AFM in the bulk to canted ferrimagnetic or 4-sublattice AFM at the surface.

Single crystal Cr_2O_3 . Bulk chromia belongs to the magnetic symmetry point group $\bar{3}'m'$ that includes 3-fold and 2-fold rotation axes and the center of anti-inversion (i.e., inversion center with time inversion) [Fig. 1(b)]. In Cr_2O_3 , the bulk energy of the uniform state $\mathbf{L} = \{L_x, L_y, L_z\} = \text{const}$ is $w_{\text{bulk}} = \lambda M^2 - K L_z^2$ [10] (supplemental material [33], Sec. I), where λ is the constant of the uniform exchange, and $K > 0$ is the anisotropy constant. Here and in the following, $\hat{\mathbf{z}}$ is the direction parallel to the c axis. The high-symmetry c -plane cut of chromia has a finite magnetization originating from non-relativistic exchange, which is proportional to the sublattice

magnetization [7, 8].

To determine the magnetic state of a semi-infinite slab with the surface of a given crystallographic cut, one should complement w_{bulk} by the surface energy density w_s . In the following, we will focus on the m plane and a plane surfaces, which have an in-plane magnetic easy axis. The allowed components of magnetization on a surface are determined by the subset of bulk symmetry operations that keep the direction of the surface normal invariant [7, 18, 34].

Surface magnetism of m -plane Cr_2O_3 . We first discuss the magnetism on the m -plane of chromia, which possesses the magnetic symmetry group m' [Fig. 1(c)]. The mirror plane coupled to time-reversal m' transforms μ_1 into μ_3 (μ_2 into μ_4) which belong to the same AFM sublattices. This changes the surface symmetry of m -plane chromia to that of a *ferrimagnet* rather than of an AFM [35]. We determine the surface energy density w_{bulk} as the scalar function that is a sum of bilinear and quadratic forms on components of \mathbf{M} and \mathbf{L} and is invariant under m' . For the m plane it is given by

$$w_s^m = \lambda_s M^2 + D(\mathbf{M} \cdot \mathbf{L}) + D_{xz} M_x L_z + D_{zx} M_z L_x. \quad (1)$$

Here, $\hat{\mathbf{x}}$ is the direction parallel to the surface normal, and λ_s is the constant of the uniform exchange at the surface, which is of the order of λ . Coefficients D , D_{xz} and D_{zx} correspond to the surface-symmetry-driven homogenous Dzyaloshinskii terms which are absent in bulk Cr_2O_3 because coupling between \mathbf{M} and \mathbf{L} is forbidden for the $\bar{3}'m'$ symmetry group. Their microscopic origin can be determined by considering the spin Hamiltonian with single- and inter-ion anisotropies and antisymmetric exchange ([33], Sec. I.C). The term with coefficient D originates from the single-ion anisotropy and is responsible for the emergent ferrimagnetism. Coefficients

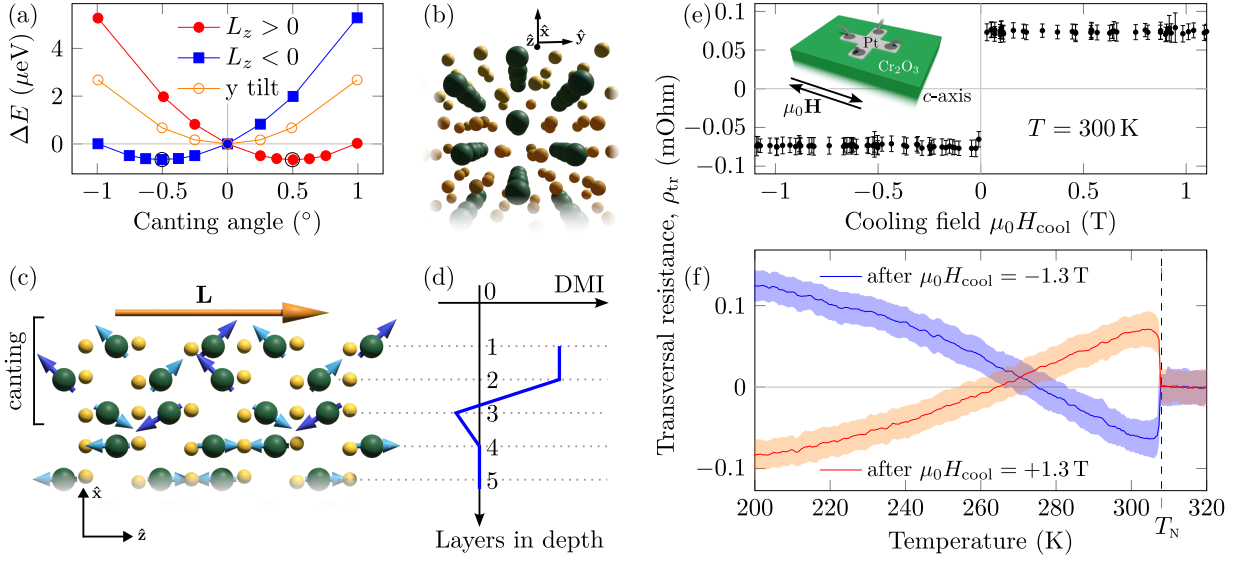


FIG. 2. *m*-plane Cr_2O_3 surface. (a) Calculated change in energy per surface as a function of canting angle for both directions of the Néel vector \mathbf{L} . Positive (negative) canting corresponds to an out-of-plane magnetization toward vacuum (bulk). The energy minima for canting along $\hat{\mathbf{x}}$ are indicated by black circles. (b) Side view of the Cr_2O_3 slab in DFT simulations and (c) its front view with arrows indicating the direction of magnetic moments. The Néel vector \mathbf{L} is shown by the yellow arrow. (d) Schematics of the change in effective DMI per layer. (e) Experimentally measured spontaneous transversal resistance vs cooling magnetic field. Inset shows schematic of the setup. (f) Measured change of the transversal resistance during zero field warming after cooling in positive and negative fields (red and blue lines, respectively). Fade regions around lines indicate standard deviation of the data. Dashed line indicates the Néel temperature $T_N = 308$ K.

$D_{xz} = D_{\text{sym}} + D_{\text{asym}}$ and $D_{zx} = D_{\text{sym}} - D_{\text{asym}}$ quantify the spin canting at the surface. The symmetric term D_{sym} stems from the single-ion anisotropy, while the asymmetric term D_{asym} consists of contributions from the inter-ion anisotropy and antisymmetric exchange.

The equilibrium state, determined by the energy minimum for w_{bulk} and w_s^m , corresponds to

$$\mathbf{L} = L_z \hat{\mathbf{z}}, \quad \mathbf{M} = -\frac{L_z}{2\lambda_s} \{D_{xz}, 0, D\} + \mathcal{O}(\lambda^{-2}). \quad (2)$$

Thus, the *m* plane cut behaves as a canted ferrimagnet with the magnetization in the *xz* plane uniquely determined by the bulk ground state \mathbf{L} . We stress that the presence of relativistic terms in Eq. (1) leading to $\mathbf{M} \neq 0$ in (2) makes the *m*-plane surface qualitatively distinct from the *c* plane of Cr_2O_3 , where the surface magnetization is due to exchange [7, 9, 34] (see also [33], Sec. I.A).

Constrained magnetic calculations within density functional theory (DFT) ([33], Sec. II) [18] confirm that the vacuum-terminated surface of the *m*-plane Cr_2O_3 having $M_x, M_z \neq 0$ is energetically favorable compared to an *m*-plane surface with $M_x = M_z = 0$, consistent with a surface magnetization of the form of Eq. (2). We fix Cr magnetic moments in the center two layers of a four-layer vacuum-terminated slab of Cr_2O_3 with an *m*-plane surface to lie completely along the bulk Néel vector ([001] crystallographic direction) with the ground state magnetic ordering. On the top and bottom outermost surface layers, we induce a surface magnetization by constrain-

ing the Cr moments to cant with equal angles along the surface normal, while allowing their magnitudes along L_z to vary [Fig. 2(a)]. The canting angle is defined with respect to the L_z [001] direction and we define positive angles as canting toward vacuum, and negative as moments canting toward the bulk.

In Fig. 2(a) we plot the change in total energy per formula unit with respect to energy at 0° canting ($M_x = 0$) as function of the canting angle. We perform two sets of calculations, corresponding to the two bulk AFM domains with $L_z > 0$ and $L_z < 0$. In line with the symmetry analysis, the DFT data in Fig. 2(a) demonstrate that the energy minimum corresponds to a finite canting angle of around $+0.5^\circ$ (-0.5°) for $L_z > 0$ ($L_z < 0$). The canting results in an induced out-of-plane magnetization of about $+0.1\mu_B$ ($-0.1\mu_B$) for every four Cr surface moments within the bulk unit cell. The in-plane ferrimagnetic magnetization M_z is smaller than M_x by about a factor of two. Furthermore, we study spin canting in sub-surface layers [Fig. 2(b) and [33] Sec. II]. The second layer of Cr ions reveals roughly the same magnitude of M_x and M_z as the topmost layer while the third layer of ions reveals a small canting of order of 0.1° in the opposite direction [Fig. 2(c,d)].

The values of spin canting obtained from DFT allow us to quantify the DMI and other material parameters in Eq. (1) for low temperatures, see Supplementary Table II ([33], Sec. III). The degree of ferrimagnetic asymmetry between magnetic sublattices is deter-

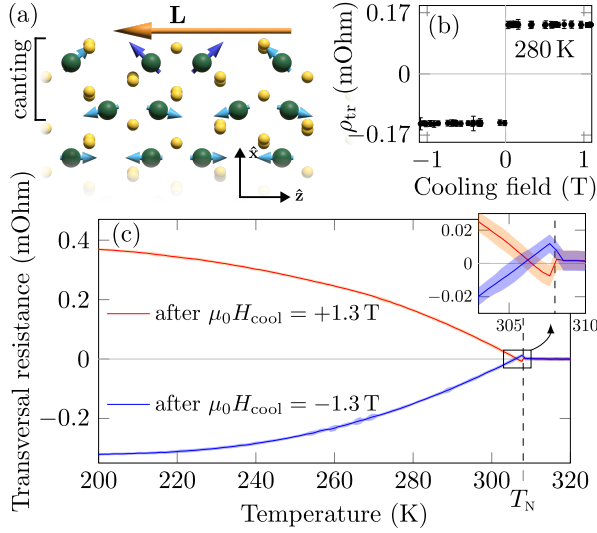


FIG. 3. *a*-plane Cr_2O_3 surface. (a) Front view of the slab used in DFT simulations with arrows indicating the direction of magnetic moments. (b) Measured spontaneous transversal resistance vs cooling magnetic field. (c) Change of the transversal resistance measured during zero field warming after cooling in positive and negative fields (red and blue lines, respectively). Fade regions around lines indicate standard deviation of the data. Dashed line indicates the Néel temperature $T_N = 308$ K.

mined by $D \approx 0.5 \times 10^{-15} \text{ T}^2 \text{ m}^4 / \text{J}$. The inequality of the off-diagonal coefficients $D_{xz} \approx 1 \times 10^{-15} \text{ T}^2 \text{ m}^4 / \text{J}$ and $D_{zx} \approx 3 \times 10^{-15} \text{ T}^2 \text{ m}^4 / \text{J}$ indicate that both symmetric and antisymmetric components of the DMI are sizeable. The estimated values of DMI can be compared with other materials by normalizing relative to the sublattice magnetization $M_0 \approx 5 \times 10^5 \text{ A/m}$ [36]. Then, $\tilde{D}_{xz} = D_{xz} / (4M_0^2) \approx 1 \text{ mJ/m}^2$. This value is of the same order as the interfacial DMI in asymmetric Co sandwiches [37, 38] and the values reported for yttrium iron garnets with asymmetric interfaces [39]. The physical consequence of the surface-symmetry-driven DMI is the coupling between the surface magnetization and the bulk order parameter.

To verify the presence of coupling between \mathbf{M} and \mathbf{L} , we perform magnetotransport measurements of a 3-nm-thick Pt thin film prepared on the m plane of a Cr_2O_3 single crystal [inset in Fig. 2(e), [33], Sec. IV,V]. The sample is cooled from 325 K (above T_N) to the temperature of interest in an applied magnetic field \mathbf{H}_{cool} oriented along the chromia c axis. This field cooling protocol assures unique selection of a single AFM domain in the sample, fixing the direction of the bulk Néel vector \mathbf{L} [40, 41]. Subsequently, the magnetic field is lowered to zero and the transversal resistance is measured at remanence. We determine that the transversal resistance ρ_{tr} changes sign with the polarity of the cooling field [Fig. 2(e)]. This indicates that the orientation of the out-of-plane component

of the surface magnetization M_x at the m plane Cr_2O_3 is linked to the bulk \mathbf{L} . Although the physical origin of the out-of-plane magnetization at the surface of m plane is different than that of c plane chromia (relativistic vs. exchange), the experimental fingerprint is similar. Namely, the sign of the transversal resistance ρ_{tr} is sensitive to the sign of the interfacial M_x [13, 23]. In the paramagnetic state ($T > T_N$), transversal resistances measured in positive and negative cooling fields are equal, $\rho_{\text{tr}}^+ = \rho_{\text{tr}}^-$ [Fig. 2(f)].

In contrast to the established magnetotransport studies of c -plane chromia, where transversal resistance changes monotonically with temperature [23, 42–45], ([33], Sec. V), the measured ρ_{tr} of the m -plane sample is not monotonic. In particular, we observe a crossover of the two curves at $T_m \approx 270$ K which is evidence of the change of the magnetization sign at the surface [Fig. 2(f)]. Our Monte Carlo simulations show that weakening of the exchange bonds at the surface does not lead to the reduction of T_N for the surface layer of moments ([33], Sec. VI). Thus, it is unlikely that the reversal of the magnetization sign is related to transition of the first two layers of Cr to a paramagnetic state and domination of the contribution of the third layer of moments which has the opposite direction [Fig. 2(c,d)]. We attribute the crossover to the temperature dependence of the DMI, specifically, the different temperature scalings of the single-ion anisotropy determining D_{sym} and the antisymmetric exchange with the inter-ion anisotropy determining D_{asym} ([33], Sec. VI).

Surface magnetism of a-plane Cr_2O_3 . We perform the same theoretical and experimental analysis for another nominally magnetically compensated crystallographic cut of Cr_2O_3 , the a plane [Fig. 1(d) ([33], Sec. I.C)], which belongs to the magnetic point symmetry group 2 having only the two-fold rotation axis. The surface magnetic energy density determined by the symmetry considerations in the same way as for the m plane is given by

$$w_s^a = \lambda_s M^2 + D_{xy} M_x L_y + D_{yx} M_y L_x + D_{xz} M_x L_z + D_{zx} M_z L_x, \quad (3)$$

with the corresponding ground state magnetic order given by

$$\mathbf{L} = L_z \hat{\mathbf{z}}, \quad \mathbf{M} = - \left\{ \frac{D_{xz}}{2\lambda_s} L_z, 0, 0 \right\} + \mathcal{O}(\lambda^{-2}), \quad (4)$$

where the $\hat{\mathbf{x}}$ axis points along the a plane surface normal. The 2-fold rotation in the a -plane surface point group maps moments $\boldsymbol{\mu}_1$ and $\boldsymbol{\mu}_3$ into opposite AFM sublattices $\boldsymbol{\mu}_2$ and $\boldsymbol{\mu}_4$. Thus, the a plane surface cut of Cr_2O_3 behaves as the four-sublattice weak ferromagnet, while the bulk remains a collinear two-sublattice AFM. The weak ferromagnetism at the surface of the chromia a -plane is determined by the surface-symmetry-driven DMI term D_{xz} .

In contrast to the m plane where we observed finite spin canting for the top three layers, DFT calculations for the a plane ([33], Sec. II) reveal that spin canting is present only for the first two layers of magnetic moments [Fig. 3(a)]. The value of spin canting angle allows us to estimate $D_{xz} \approx -0.6 \times 10^{-15} \text{ T}^2 \text{ m}^4 / \text{J}$ ([33], Sec. III). In line with the theoretical predictions, magnetotransport measurements [Fig. 3(b,c)] ([33], Sec. V) indicate the presence of out-of-plane surface magnetization whose sign is reversed upon reversing \mathbf{L} . The calculated canting angle corresponding to the energy minimum for the a plane is about half that for the m plane. A crucial difference between the a plane and m plane is that the sign of the equilibrium surface magnetization predicted by DFT is opposite for a fixed sign of \mathbf{L} [for the a plane, $L_z < 0$ corresponds to positive M_x , see Fig. 3(a)]. This effect is also captured experimentally, reflected in the opposite sign of the transversal resistance measured for the a -plane and m -plane samples after identical field cooling protocols [c.f. Fig. 2(f) and Fig. 3(c)]. Similarly to the m -plane case, a crossover of the ρ_{tr}^{\pm} curves is observed for the a plane although the crossover temperature, $T_a \approx 306 \text{ K}$, is closer to T_N [Fig. 3(c)]. The crossover in the a -plane temperature dependence suggests that the crossover phenomenon cannot be related to a ferrimagnetic compensation point because the a -plane surface of chromia is not ferrimagnetic.

Discussion. The combination of the symmetry analysis and DFT calculations presented here can be straightforwardly extended to other systems and applied for the analysis of non-collinear magnetic textures. The latter involves the additional consideration of inhomogeneous DMI terms including derivatives of the magnetic vectors. The distinction between bulk and surface magnetic states could alter interfacial phenomena such as spin pumping [14, 46, 47]. Our findings could be further applied for analysis of the surface responses considering features of multisublattice behavior of AFMs [48] as well as ferrimagnet-specific solitons [49–51].

To summarise, we describe the surface-symmetry-driven DMI at nominally compensated surfaces of chromia. This strong DMI of $\sim 1 \text{ mJ/m}^2$ causes new physical effects at this otherwise collinear magnetoelectric AFM including (i) sizeable ($\sim 0.5^\circ$) spin canting at the surface, with the direction uniquely determined by the bulk Néel vector, (ii) change of the magnetic ordering at the surface from AFM to ferrimagnetic, and (iii) peculiar temperature dependence of the magnetotransport.

Our findings provide new insight into the physics of antiferromagnetic material surfaces and expand their technological potential. In particular, the possibility to assess the Néel state of in-plane easy axis AFM surfaces in conventional magnetotransport measurements is crucial for low-energy magnetic data storage [1, 52] and logic [53] devices. Furthermore, the experimentally demonstrated all-electric readout of the state of these AFMs can link

spintronics and AFM magnonics, which relies on the long range propagation of spin waves in AFMs with in-plane easy axes [6, 54]. The unusual temperature dependency of the surface magnetization allows control of the sign of the surface magnetization with heating while keeping the bulk antiferromagnetic state. Our work positions the m and a planes of chromia as promising materials science platforms for studies of long-range magnon propagation and spin superfluidity.

Acknowledgements. We thank Dr. Tobias Kosub (HZDR Innovation GmbH) for insightful discussions on magnetotransport data of chromia. This work is financed in part via the German Research Foundation (DFG) under Grants No. MA 5144/22-1, MA 5144/24-1, MA 5144/33-1 and and via European Union in the frame of the project REGO (ID: 101070066). S.F.W. and N.A.S. were supported by the ERC under the European Union’s Horizon 2020 research and innovation programme with grant No. 810451, and by ETH Zürich. Computational resources for the DFT calculations were provided by the Swiss National Supercomputing Centre (CSCS) under project number s1128 and by ETH Zürich’s EULER cluster.

* o.pylypovskyi@hzdr.de; These authors contributed equally

† sophie.weber@mat.ethz.ch; These authors contributed equally

‡ nicola.spaldin@mat.ethz.ch

§ d.makarov@hzdr.de

- [1] T. Kosub, M. Kopte, R. Hühne, P. Appel, B. Shields, P. Maletinsky, R. Hübner, M. O. Liedke, J. Fassbender, O. G. Schmidt, and D. Makarov, Purely antiferromagnetic magnetoelectric random access memory, *Nature Communications* **8**, 13985 (2017).
- [2] A. Mahmood, W. Echtenkamp, M. Street, J.-L. Wang, S. Cao, T. Komesu, P. A. Dowben, P. Buragohain, H. Lu, A. Gruverman, A. Parthasarathy, S. Rakheja, and C. Binek, Voltage controlled Néel vector rotation in zero magnetic field, *Nature Communications* **12**, 1674 (2021).
- [3] N. Hedrich, K. Wagner, O. V. Pylypovskyi, B. J. Shields, T. Kosub, D. D. Sheka, D. Makarov, and P. Maletinsky, Nanoscale mechanics of antiferromagnetic domain walls, *Nature Physics* **17**, 574 (2021).
- [4] J. Li, C. B. Wilson, R. Cheng, M. Lohmann, M. Kavand, W. Yuan, M. Aldosary, N. Agladze, P. Wei, M. S. Sherwin, and J. Shi, Spin current from sub-terahertz-generated antiferromagnetic magnons, *Nature* **578**, 70 (2020).
- [5] P. Makushko, T. Kosub, O. V. Pylypovskyi, N. Hedrich, J. Li, A. Pashkin, S. Avdoshenko, R. Hübner, F. Ganss, D. Wolf, A. Lubk, M. O. Liedke, M. Butterling, A. Wagner, K. Wagner, B. J. Shields, P. Lehmann, I. Veremchuk, J. Fassbender, P. Maletinsky, and D. Makarov, Flexomagnetism and vertically graded Néel temperature of antiferromagnetic Cr_2O_3 thin films, *Nature Communications* **13**, 6745 (2022).

- [6] W. Yuan, Q. Zhu, T. Su, Y. Yao, W. Xing, Y. Chen, Y. Ma, X. Lin, J. Shi, R. Shindou, X. C. Xie, and W. Han, Experimental signatures of spin superfluid ground state in canted antiferromagnet Cr_2O_3 via nonlocal spin transport, *Science Advances* **4**, eaat1098 (2018).
- [7] K. D. Belashchenko, Equilibrium magnetization at the boundary of a magnetoelectric antiferromagnet, *Physical Review Letters* **105**, 147204 (2010).
- [8] S. F. Weber and N. A. Spaldin, Characterizing and overcoming surface paramagnetism in magnetoelectric antiferromagnets, *Physical Review Letters* **130**, 146701 (2023).
- [9] A. F. Andreev, Macroscopic magnetic fields of antiferromagnets, *Journal of Experimental and Theoretical Physics Letters* **63**, 758 (1996).
- [10] I. E. Dzialoshinskii, Thermodynamic theory of “weak” ferromagnetism in antiferromagnetic substances, *Sov. Phys. JETP* **5**, 1259 (1957).
- [11] T. Moriya, New mechanism of anisotropic superexchange interaction, *Physical Review Letters* **4**, 228 (1960).
- [12] S. Mu and K. D. Belashchenko, Influence of strain and chemical substitution on the magnetic anisotropy of antiferromagnetic Cr_2O_3 : An ab-initio study, *Physical Review Materials* **3**, 034405 (2019).
- [13] T. Iino, T. Moriyama, H. Iwaki, H. Aono, Y. Shiratsuchi, and T. Ono, Resistive detection of the Néel temperature of Cr_2O_3 thin films, *Applied Physics Letters* **114**, 022402 (2019).
- [14] R. Rodriguez, S. Regmi, H. Zhang, W. Yuan, P. Makushko, E. A. Montoya, I. Veremchuk, R. Hübner, D. Makarov, J. Shi, R. Cheng, and I. Barsukov, Robust spin injection via thermal magnon pumping in antiferromagnet/ferromagnet hybrid systems, *Physical Review Research* **4**, 033139 (2022).
- [15] A. Erickson, S. Q. Abbas Shah, A. Mahmood, I. Fescenko, R. Timalisina, C. Binek, and A. Laraoui, Nanoscale imaging of antiferromagnetic domains in epitaxial films of Cr_2O_3 via scanning diamond magnetic probe microscopy, *RSC Advances* **13**, 178 (2023).
- [16] K. Du, X. Xu, C. Won, K. Wang, S. A. Crooker, S. Rangan, R. Bartynski, and S.-W. Cheong, Topological surface magnetism and Néel vector control in a magnetoelectric antiferromagnet, *npj Quantum Materials* **8**, 17 (2023).
- [17] Y.-H. Lai, P.-W. Shao, C.-Y. Kuo, C.-E. Liu, Z. Hu, C. Luo, K. Chen, F. Radu, Y.-J. Wang, J. Zheng, C. Duan, C.-F. Chang, L. Chang, Y.-C. Chen, S.-W. Cheong, and Y.-H. Chu, Quasi-static modulation of multiferroic properties in flexible magnetoelectric Cr_2O_3 /muscovite heteroepitaxy, *Acta Materialia* **243**, 118509 (2023).
- [18] S. F. Weber, A. Urru, S. Bhowal, C. Ederer, and N. A. Spaldin, Surface magnetization in antiferromagnets: Classification, example materials, and relation to magnetoelectric responses, *ArXiv e-prints* (2023).
- [19] M. S. Wörnle, P. Welter, M. Giraldo, T. Lottermoser, M. Fiebig, P. Gambardella, and C. L. Degen, Coexistence of Bloch and Néel walls in a collinear antiferromagnet, *Physical Review B* **103**, 094426 (2021).
- [20] F. Casola, T. van der Sar, and A. Yacoby, Probing condensed matter physics with magnetometry based on nitrogen-vacancy centres in diamond, *Nature Reviews Materials* **3**, 17088 (2018).
- [21] W. S. Huxter, M. L. Palm, M. L. Davis, P. Welter, C.-H. Lambert, M. Trassin, and C. L. Degen, Scanning gradiometry with a single spin quantum magnetometer, *Nature Communications* **13**, 3761 (2022).
- [22] P. Schoenherr, L. Giraldo, M. Lilienblum, M. Trassin, D. Meier, and M. Fiebig, Magnetoelectric force microscopy on antiferromagnetic 180° domains in Cr_2O_3 , *Materials* **10**, 1051 (2017).
- [23] T. Kosub, M. Koppe, F. Radu, O. G. Schmidt, and D. Makarov, All-electric access to the magnetic-field-invariant magnetization of antiferromagnets, *Physical Review Letters* **115**, 097201 (2015).
- [24] Y. Shiratsuchi, K. Toyoki, and R. Nakatani, Magnetoelectric control of antiferromagnetic domain state in Cr_2O_3 thin film, *Journal of Physics: Condensed Matter* **33**, 243001 (2021).
- [25] K. Ujimoto, H. Sameshima, K. Toyoki, Y. Kotani, T. Moriyama, K. Nakamura, R. Nakatani, and Y. Shiratsuchi, Direct observation of antiferromagnetic domains and field-induced reversal in $\text{Pt}/\text{Cr}_2\text{O}_3/\text{Pt}$ epitaxial trilayers, *Applied Physics Letters* **123**, 022407 (2023).
- [26] A. Mahmood, J. Weaver, S. Q. A. Shah, W. Echtenkamp, J. W. Lynn, P. A. Dowben, and C. Binek, Post deposition interfacial Néel temperature tuning in magnetoelectric $\text{B:Cr}_2\text{O}_3$, *ArXiv e-prints* 10.48550/arXiv.2309.12493 (2023).
- [27] S. Shi, A. L. Wysocki, and K. D. Belashchenko, Magnetism of chromia from first-principles calculations, *Physical Review B* **79**, 104404 (2009).
- [28] M. Mostovoy, A. Scaramucci, N. A. Spaldin, and K. T. Delaney, Temperature-dependent magnetoelectric effect from first principles, *Physical Review Letters* **105**, 087202 (2010).
- [29] M. Fechner, A. Sukhov, L. Chotorlishvili, C. Kenel, J. Berakdar, and N. A. Spaldin, Magnetophonics: Ultrafast spin control through the lattice, *Physical Review Materials* **2**, 064401 (2018).
- [30] A. N. Bogdanov and D. A. Yablonskii, Thermodynamically stable “vortices” in magnetically ordered crystals. The mixed state of magnets, *Zh. Eksp. Teor. Fiz.* **95**, 178 (1989).
- [31] A. Fert, N. Reyren, and V. Cros, Magnetic skyrmions: advances in physics and potential applications, *Nature Reviews Materials* **2**, 17031 (2017).
- [32] Thus, it takes into account the inversion symmetry break at the sample’s interface.
- [33] Supplemental material [link provided by publisher] also cites [3, 7–10, 12, 18, 27, 34, 36, 55–74].
- [34] V. I. Marchenko, Exchange effects at the boundaries of magnets, *Sov. Phys. JETP* **53**, 1045 (1981).
- [35] Mathematical definition of an AFM requires the symmetry operation in magnetic point symmetry group, which transforms sublattices into each other, which makes them distinct from ferrimagnets at the compensation point [75].
- [36] E. Samuelsen, M. Hutchings, and G. Shirane, Inelastic neutron scattering investigation of spin waves and magnetic interactions in Cr_2O_3 , *Physica* **48**, 13 (1970).
- [37] O. Boulle, J. Vogel, H. Yang, S. Pizzini, D. de Souza Chaves, A. Locatelli, T. O. Mentes, A. Sala, L. D. Buda-Prejbeanu, O. Klein, M. Belmeguenai, Y. Roussigné, A. Stashkevich, S. M. Chérif, L. Aballe, M. Foerster, M. Chshiev, S. Auffret, I. M. Miron, and G. Gaudin, Room-temperature chiral magnetic skyrmions in ultrathin magnetic nanostructures,

- Nature Nanotech **11**, 449 (2016).
- [38] O. M. Volkov, F. Kronast, C. Abert, E. S. O. Mata, T. Kosub, P. Makushko, D. Erb, O. V. Pylypovskyi, M.-A. Mawass, D. Sheka, S. Zhou, J. Fassbender, and D. Makarov, Domain-wall damping in ultrathin nanostripes with Dzyaloshinskii-Moriya interaction, *Physical Review Applied* **15**, 034038 (2021).
 - [39] H. Wang, J. Chen, T. Liu, J. Zhang, K. Baumgaertl, C. Guo, Y. Li, C. Liu, P. Che, S. Tu, S. Liu, P. Gao, X. Han, D. Yu, M. Wu, D. Grundler, and H. Yu, Chiral spin-wave velocities induced by all-garnet interfacial Dzyaloshinskii-Moriya interaction in ultrathin yttrium iron garnet films, *Physical Review Letters* **124**, 027203 (2020).
 - [40] P. J. Brown, J. B. Forsyth, and F. Tasset, A study of magnetoelectric domain formation in Cr_2O_3 , *Journal of Physics: Condensed Matter* **10**, 663 (1998).
 - [41] T. Ashida, M. Oida, N. Shimomura, T. Nozaki, T. Shibata, and M. Sahashi, Observation of magnetoelectric effect in $\text{Cr}_2\text{O}_3/\text{Pt}/\text{Co}$ thin film system, *Applied Physics Letters* **104**, 152409 (2014).
 - [42] Y. Ji, J. Miao, Y. M. Zhu, K. K. Meng, X. G. Xu, J. K. Chen, Y. Wu, and Y. Jiang, Negative spin hall magnetoresistance in antiferromagnetic $\text{Cr}_2\text{O}_3/\text{Ta}$ bilayer at low temperature region, *Applied Physics Letters* **112**, 232404 (2018).
 - [43] R. Schlitz, T. Kosub, A. Thomas, S. Fabretti, K. Nielsch, D. Makarov, and S. T. B. Goennenwein, Evolution of the spin Hall magnetoresistance in $\text{Cr}_2\text{O}_3/\text{Pt}$ bilayers close to the Néel temperature, *Applied Physics Letters* **112**, 132401 (2018).
 - [44] T. Moriyama, Y. Shiratsuchi, T. Iino, H. Aono, M. Suzuki, T. Nakamura, Y. Kotani, R. Nakatani, K. Nakamura, and T. Ono, Giant anomalous hall conductivity at the $\text{Pt}/\text{Cr}_2\text{O}_3$ interface, *Physical Review Applied* **13**, 034052 (2020).
 - [45] X. Wang, K. Toyoki, R. Nakatani, and Y. Shiratsuchi, Magnetic-field and temperature dependence of anomalous Hall effect in $\text{Pt}/\text{Cr}_2\text{O}_3/\text{Pt}$ trilayer, *AIP Advances* **12**, 10.1063/9.0000253 (2022).
 - [46] S. Schlauderer, C. Lange, S. Baierl, T. Ebnet, C. P. Schmid, D. C. Valovcin, A. K. Zvezdin, A. V. Kimel, R. V. Mikhaylovskiy, and R. Huber, Temporal and spectral fingerprints of ultrafast all-coherent spin switching, *Nature* **569**, 383 (2019).
 - [47] C. Liu, Y. Luo, D. Hong, S. S.-L. Zhang, H. Saglam, Y. Li, Y. Lin, B. Fisher, J. E. Pearson, J. S. Jiang, H. Zhou, J. Wen, A. Hoffmann, and A. Bhattacharya, Electric field control of magnon spin currents in an antiferromagnetic insulator, *Science Advances* **7**, 10.1126/sciadv.abg1669 (2021).
 - [48] A. G. Gurevich and G. A. Melkov, *Magnetization Oscillations and Waves* (CRC PR INC, 2000).
 - [49] B. A. Ivanov, Ultrafast spin dynamics and spintronics for ferrimagnets close to the spin compensation point (review), *Low Temperature Physics* **45**, 935 (2019).
 - [50] E. Galkina, N. Kulagin, and B. A. Ivanov, Dynamics of Dzyaloshinskii domain walls for ferrimagnets with compensation of angular momentum, *Annals of Physics* **447**, 169080 (2022).
 - [51] C. E. Zaspel, E. G. Galkina, and B. A. Ivanov, Ferrimagnetic magnon drop solitons close to the angular momentum compensation point, *Physical Review B* **108**, 064403 (2023).
 - [52] X. He, Y. Wang, N. Wu, A. N. Caruso, E. Vescovo, K. D. Belashchenko, P. A. Dowben, and C. Binek, Robust isothermal electric control of exchange bias at room temperature, *Nature Materials* **9**, 579 (2010).
 - [53] S. Manipatruni, D. E. Nikonov, C.-C. Lin, T. A. Gosavi, H. Liu, B. Prasad, Y.-L. Huang, E. Bonturim, R. Ramesh, and I. A. Young, Scalable energy-efficient magnetoelectric spin-orbit logic, *Nature* **565**, 35 (2018).
 - [54] A. Ross, R. Lebrun, O. Gomonay, D. A. Grave, A. Kay, L. Baldrati, S. Becker, A. Qaiumzadeh, C. Ulloa, G. Jakob, F. Kronast, J. Sinova, R. Duine, A. Brataas, A. Rothschild, and M. Kläui, Propagation length of antiferromagnetic magnons governed by domain configurations, *Nano Letters* **20**, 306 (2020).
 - [55] K. Siratori, K. Kohn, and E. Kita, Magnetoelectric effect in magnetic materials, *Acta Physica Polonica A* **81**, 431 (1992).
 - [56] G. Kresse and J. Furthmüller, Efficient iterative schemes for *ab initio* total-energy calculations using a plane-wave basis set, *Physical Review B* **54**, 11169 (1996).
 - [57] P. E. Blöchl, Projector augmented-wave method, *Physical Review B* **50**, 17953 (1994).
 - [58] V. I. Anisimov, F. Aryasetiawan, and A. I. Lichtenstein, First-principles calculations of the electronic structure and spectra of strongly correlated systems: the LDA+U method, *Journal of Physics: Condensed Matter* **9**, 767 (1997).
 - [59] S. L. Dudarev, G. A. Botton, S. Y. Savrasov, C. J. Humphreys, and A. P. Sutton, Electron-energy-loss spectra and the structural stability of nickel oxide: An LSDA+U study, *Physical Review B* **57**, 1505 (1998).
 - [60] P.-W. Ma and S. L. Dudarev, Constrained density functional for noncollinear magnetism, *Physical Review B* **91**, 054420 (2015).
 - [61] Y. Kota and H. Imamura, Narrowing of antiferromagnetic domain wall in corundum-type Cr_2O_3 by lattice strain, *Applied Physics Express* **10**, 013002 (2017).
 - [62] I. Veremchuk, P. Makushko, N. Hedrich, Y. Zabala, T. Kosub, M. O. Liedke, M. Butterling, A. G. Attallah, A. Wagner, U. Burkhardt, O. V. Pylypovskyi, R. Hübner, J. Fassbender, P. Maletinsky, and D. Makarov, Magnetism and magnetoelectricity of textured polycrystalline bulk Cr_2O_3 sintered in conditions far out of equilibrium, *ACS Applied Electronic Materials* **4**, 2943 (2022).
 - [63] A. Parthasarathy and S. Rakheja, Dynamics of magnetoelectric reversal of an antiferromagnetic domain, *Physical Review Applied* **11**, 034051 (2019).
 - [64] A. Hoser and U. Köbler, *Renormalization Group Theory* (Springer Berlin Heidelberg, 2012).
 - [65] S. Foner, High-field antiferromagnetic resonance in Cr_2O_3 , *Physical Review* **130**, 183 (1963).
 - [66] D. N. Astrov, Magnetoelectric effect in chromium oxide, *Soviet Physics JETP [J. Exp. Theor. Fiz.]* **40**, 1035 (1961) **13**, 729 (1961).
 - [67] A. S. Borovik-Romanov and H. Grimmer, Magnetic properties, in *International Tables for Crystallography* (International Union of Crystallography, Chester, England, 2006) pp. 105–149.
 - [68] A. H. Morrish, *Canted antiferromagnetism: Hematite* (1995).
 - [69] M. Al-Mahdawi, S. P. Pati, Y. Shiokawa, S. Ye, T. Nozaki, and M. Sahashi, Low-energy magnetoelectric control of domain states in exchange-coupled heterostruc-

- tures, *Physical Review B* **95**, 144423 (2017).
- [70] E. V. Gomonay and V. M. Loktev, On the theory of the formation of equilibrium domain structure in antiferromagnets, *Low Temperature Physics* **30**, 804 (2004).
 - [71] B. Skubic, J. Hellsvik, L. Nordström, and O. Eriksson, A method for atomistic spin dynamics simulations: implementation and examples, *Journal of Physics: Condensed Matter* **20**, 315203 (2008).
 - [72] H. Callen and E. Callen, The present status of the temperature dependence of magnetocrystalline anisotropy, and the power law, *Journal of Physics and Chemistry of Solids* **27**, 1271 (1966).
 - [73] M. Tachiki and T. Nagamiya, Origin of the magnetic anisotropy energy of antiferromagnetic Cr_2O_3 , *Journal of the Physical Society of Japan* **13**, 452 (1958).
 - [74] Y. Zhang, X. Kong, G. Xu, Y. Jin, C. Jiang, and G. Chai, Direct observation of the temperature dependence of Dzyaloshinskii-Moriya interaction, *Journal of Physics D: Applied Physics* **55**, 195304 (2022).
 - [75] B. A. Ivanov, Mesoscopic antiferromagnets: statics, dynamics, and quantum tunneling (Review), *Low Temperature Physics* **31**, 635 (2005).